Multiple-band transmission of acoustic wave through metallic gratings

Dong-Xiang Qi, Ren-Hao Fan, Ru-Wen Peng, Xian-Rong Huang, Ming-Hui Lu et al.

Citation: Appl. Phys. Lett. **101**, 061912 (2012); doi: 10.1063/1.4742929
View online: http://dx.doi.org/10.1063/1.4742929
View Table of Contents: http://apl.aip.org/resource/1/APPLAB/v101/i6
Published by the American Institute of Physics.

Multiple-band transmission of acoustic wave through metallic gratings

Dong-Xiang Qi,[1] Ren-Hao Fan,[1] Ru-Wen Peng,[1,a)] Xian-Rong Huang,[2,a)] Ming-Hui Lu,[3] Xu Ni,[3] Qing Hu,[1] and Mu Wang[1,a)]
[1]*National Laboratory of Solid State Microstructures and Department of Physics, Nanjing University, Nanjing 210093, China*
[2]*Advanced Photon Source, Argonne National Laboratory, Argonne, Illinois 60439, USA*
[3]*National Laboratory of Solid State Microstructures and College of Engineering and Applied Sciences, Nanjing University, Nanjing 210093, China*

(Received 23 April 2012; accepted 24 July 2012; published online 8 August 2012)

In this work, we demonstrate that acoustic waves can achieve extremely flat transmission through a metallic grating under oblique incidence within multiple frequency bands separated by Wood's anomalies. At the low-frequency band, the transmission of acoustic wave is independent of the frequency and presents a flat curve with the transmission efficiency reaching about 100%; while at high-frequency bands, the transmission decreases to be lower flat curves due to the diffraction effect. The transmission efficiency is insensitive to the thickness of the grating. This phenomenon is verified by experiments, numerical simulations, and an analytical model. The broadband high transmission is attributed to the acoustic impedance matching between the air and the grating. This research may open up a field for various potential applications of acoustic gratings, including broadband sonic imaging and screening, grating interferometry, and antireflection cloaking. © *2012 American Institute of Physics*. [http://dx.doi.org/10.1063/1.4742929]

Metamaterials are a broad class of materials artificially engineered to exhibit unnatural and fascinating electromagnetic properties[1] that may have numerous applications, such as invisibility cloaking,[2] negative refraction,[3] deep-subwavelength focusing and imaging,[4,5] and extraordinary optical transmission (EOT).[6–13] Meanwhile, metamaterials have also been demonstrated to have analogous capabilities of manipulating acoustic waves on the subwavelength scales, thus extending their applications to acoustic wave focusing and collimation,[14] acoustic negative modulus and refraction,[15] acoustic hyperlens and imaging,[16,17] sonar sensing and screening,[18] and extraordinary acoustic transmission (EAT).[19–22] As a typical potential application, both "blinded"[23,24] and "nonblinded"[25–27] acoustic cloaking using metamaterials to route wave propagation around objects have been intensely investigated, but there is still a long way ahead since the experimental implementation must overcome the constraints that metamaterials generally suffer significant loss and narrow working frequency bands, in addition to the difficulties of nanofabrication. In fact, a simpler and more practical approach that has been used in stealth technology for low observable cloaking is to make the object antireflective by coating the surface with highly absorbing materials. However, the absorption properties of most coating materials are also frequency dependent, which makes the object still detectable by certain frequency bands.

Recently, it has been theoretically demonstrated that simple one-dimensional (1D) metallic gratings consisting of narrow slit arrays may become transparent and completely antireflective for white light (from the radio frequencies to the visible) under oblique incidence[9,28] or under normal incidence on oblique gratings,[9] and the non-dispersive transmission mechanism without resonance has been experimentally verified.[29] Very recently, broadband metamaterials are achieved for nonresonant matching of acoustic waves at a low-frequency region.[30] Here we demonstrate that 1D gratings can become transparent and largely antireflective under oblique incidence of acoustic waves within multiple frequency bands separated by Wood's anomalies. At the low-frequency band, the transmission of acoustic waves is independent of frequencies and presents a flat curve, where the transmission efficiency reaches around 100%; and at high-frequency bands, the transmission decreases to be lower flat curves due to diffraction effect. The transmission efficiency is insensitive to the thickness of the grating. The broadband transmission phenomena may have various potential applications of acoustic gratings, including broadband sonic imaging and screening,[17,18] grating interferometry, antireflection cloaking, Talbot effect-based phase contrast imaging,[31] crack detection, etc.

The first sample we studied here is a 1D periodic steel grating [see Figs. 1(a) and 1(b)]. The period and the width of the slits are $d = 4.5$ mm and $w = 1.4$ mm, respectively, and the thickness of the grating is $h = 2.76$ mm. A beam of acoustic wave is incident on the grating with a given incident angle θ. The transmission spectra were measured by an analysis package of the 3560 C Brüel & Kjær Pulse Sound and Vibration Analyzers. A 3-in. ultrasonic transducer was used as acoustic source, while a much smaller transducer was used as receiver. The zero-order transmission spectra at different incident angles were measured in the range of frequencies from 10kHz to 90kHz. The black curves in Figs. 1(c)–1(f) show the measured transmission spectra of the grating at different incident angles θ being 0° (normal incidence), 45°, 72°, and 82°, respectively. The red and blue curves correspond to simulated and analytical results, which will be discussed below. The transmission minima (marked by the arrow in Figs. 1(c)–1(f)) correspond to Wood's anomalies, where the

a)Authors to whom correspondence should be addressed. Electronic addresses: rwpeng@nju.edu.cn; xiahuang@aps.anl.gov; and muwang@nju.edu.cn.

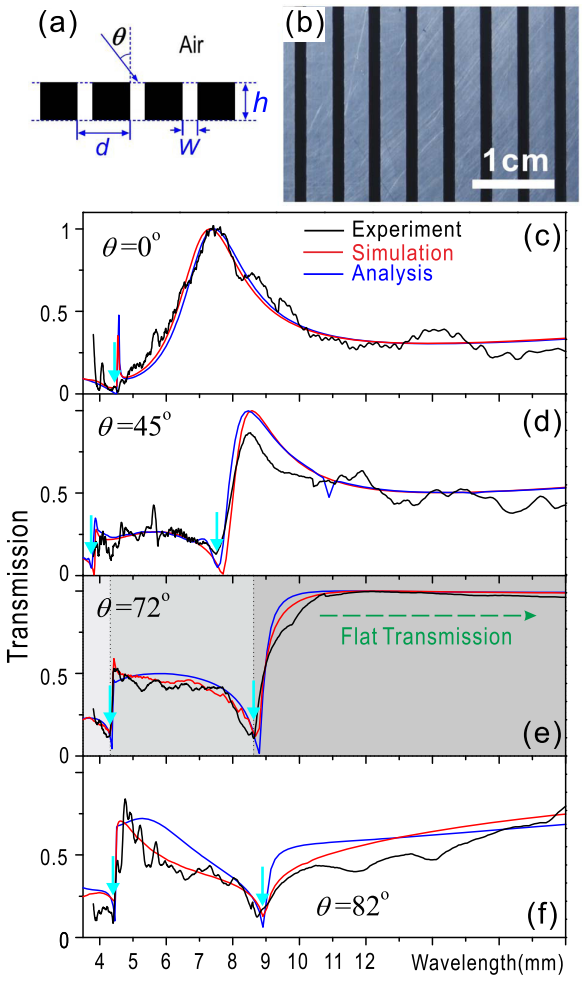

FIG. 1. (a) A schematic picture of the grating. (b) The optical image of an experimental steel grating, where the period and the width of the slits are d = 4.5 mm and w = 1.4 mm, respectively, and the thickness of the grating is h = 2.76 mm. (c)–(f) show the transmission spectra at different incident angles from the experiments (black curve), the finite-element simulation (red curve), and the analytical RCWA method (blue curve). Herein, the Wood's anomalies are marked by blue arrows. Three different gray-scale regions in Fig. 1(e) correspond to three broadband regions for flat transmission.

incident wave satisfies $d(1+\sin\theta) = n\lambda$ ($n = 1, 2, 3, \ldots$). For normal incidence ($\theta = 0°$), the transmission curve is shown in Fig. 1(c), where at the wavelength $\lambda = 7.33$ mm (i.e., $\omega = 46.8$ kHz), the main transmission peak corresponds to the well-known Fabry-Perot (FP) resonance peak.[32] There are two factors affecting the FP resonance. The first is the waveguide resonance in the slits, which is independent of the incident angle θ; the other is the coupling of waveguide modes and the diffractive waves along the grating surfaces. When θ is increased to 45° in Fig. 1(d), the FP peak still exists but has a red shift. The underlying mechanism is that with the incident angle changed, the diffractive waves are affected, which further influence the Wood's anomalies and the FP resonance peaks.

When the incident angle θ increases to 72°, as shown in Fig. 1(e), some interesting phenomena occur. (i) All the FP resonant peaks disappear. (ii) The transmission curve becomes nearly flat at multiple frequency bands separated by the Wood's anomalies as marked by different gray scales in Fig. 1(e). Especially in the long wavelength region ($\lambda = 8.8\sim19$ mm, or $\omega = 18\sim39$ kHz), which is above the first Wood's anomaly, the transmission is nearly 100%, and the grating is almost transparent for all the long wavelengths. In the shorter wavelength region between the first and the second Wood's anomalies (i.e., $\lambda = 4.34\sim8.8$ mm, or $\omega = 39\sim79$ kHz), the transmission presents a lower-level flat curve with the efficiency being about 50%. The decay of the transmission originates from that fact that the first-order diffraction wave becomes non-evanescent in this range. For even shorter wavelength region (below the second Wood's anomaly, i.e., $\lambda = 3.81\sim4.34$ mm, or $\omega = 79\sim90$ kHz), the transmission curve still keeps flat, but the efficiency further decreases to about 25% due to multiple-order diffractions. However, with θ further increased to 82°, the transmission dramatically drops (Fig. 1(f)). Therefore, we have experimentally demonstrated that metallic gratings can become highly transparent and antireflective for acoustic waves within multiple broadbands at optimal oblique incidence.

In order to study the influence of the grating thickness on the transmission for both normal- and oblique-incidence geometries, we examined another grating (sample II) with the same lattice parameter but with a different thickness h = 2.0 mm. The transmission spectra of this grating are shown in Figs. 2(c) and 2(d). For comparison, the spectra of the first grating (sample I) in Figs. 1(c) and 1(e) were replotted in Figs. 2(a) and 2(b) in terms of the frequency. As

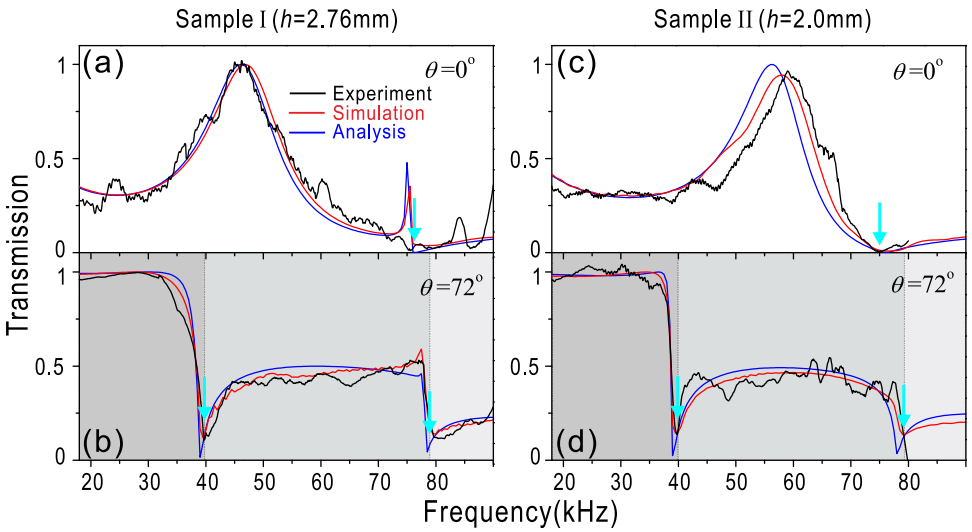

FIG. 2. Transmission spectra of two samples at both normal incidence and optimal incidence. The left panel shows the transmission spectra of sample I (the period of the slits d = 4.5 mm, the width of the slit w = 1.4 mm, and the thickness h = 2.76 mm) at different incident angles: (a) $\theta = 0°$ and (b) $\theta = 72°$. The right panel shows the transmission spectra of sample II (d = 4.5 mm, w = 1.4 mm, and h = 2.0 mm) at different incident angles: (c) $\theta = 0°$ and (d) $\theta = 72°$.

shown in Figs. 2(a) and 2(c), the transmission peak resulting from FP resonance shifts to a high frequency when the grating thickness is changed from h = 2.76 mm to 2.0 mm. This is reasonable since FP resonance strongly depends on the grating thickness. For the oblique incidence case, both the steel gratings have the same optimal incidence angle $\theta_f = 72°$. As shown in Figs. 2(b) and 2(d), under this condition, the two gratings have nearly the same maximized and flat transmission curves within multiple frequency bands. The transmission efficiency decreases with increasing acoustic frequency due to the excitation of diffraction waves. Therefore, Figure 2 shows that multiple-band flat transmission of acoustic waves is insensitive to the grating thickness.

In our study, we have utilized the finite-element simulation (using the software COMSOL MULTIPHYSICS) to calculate the zero-order transmission spectra of the two gratings, and the red curves in Figs. 1 and 2 are the calculated spectra under the corresponding experimental conditions. The good agreement between the experimental measurements and the simulations clearly show that the experiments are accurate.

In the following, we will try to explore the physical origin of multiple-band flat transmission through gratings. For sample I, although the peak transmission efficiency at $\omega = 47$ kHz for *normal incidence* [Fig. 2(a)] and the flat transmission in the $\omega = 18 \sim 39$ kHz frequency range for optimal oblique incidence [$\theta_f = 72°$, Fig. 2(b)] are both close to 100%, the calculated spatial intensity distributions of the pressure fields in Figs. 3(a) and 3(b) are obviously different. For $\omega = 47$ kHz at normal incidence, the intensity distribution in Fig. 3(a) indeed corresponds to a typical FP resonant distribution. The intensity fields inside the gating are highly confined in the slits with the intensities much larger than those of the incidence and transmitted waves outside the grating. Therefore, the transmission peak is attributed to the Fabry-Perot resonance inside the slits. However, for the flat-transmission frequency, for example, $\omega = 34$ kHz at optimal incidence of $\theta_f = 72°$, the calculated intensity field inside the slits [Fig. 3(b)] is in the same order of magnitude compared with those of the incidence and transmitted waves. Thus, the high and flat transmission under the optimal oblique incidence condition is not dominated by a resonance mechanism. Instead, it originates from the acoustic impedance matching between the effective impedance of the grating and the impedance of air, as illustrated in the following.

In order to understand the above phenomena, we have calculated the spatial distributions of the pressure fields for sample I at $\theta_f = 72°$ incidence for the frequencies $\omega = 34$ kHz, 47 kHz, and 84 kHz as shown in Figs. 3(c)–3(e), respectively. Note that these frequencies belong to three different transmission bands. For $\omega = 34$ kHz, only the zero-order transmission mode exists in Fig. 3(c) because the high-order diffractive modes are evanescent due to the sub-wavelength grating period. As a result, the incident wave energy is carried only by the propagating zero-order mode after the grating. At the frequency $\omega = 47$ kHz, the first-order diffractive mode is excited in addition to the zero-order mode, as shown in Fig. 3(d). The wave energy now is shared by the zero- and first-order modes. At $\omega = 84$ kHz, both the first- and second-order diffractive modes are exited, as shown in Fig. 3(e). Consequently, the wave energy is split

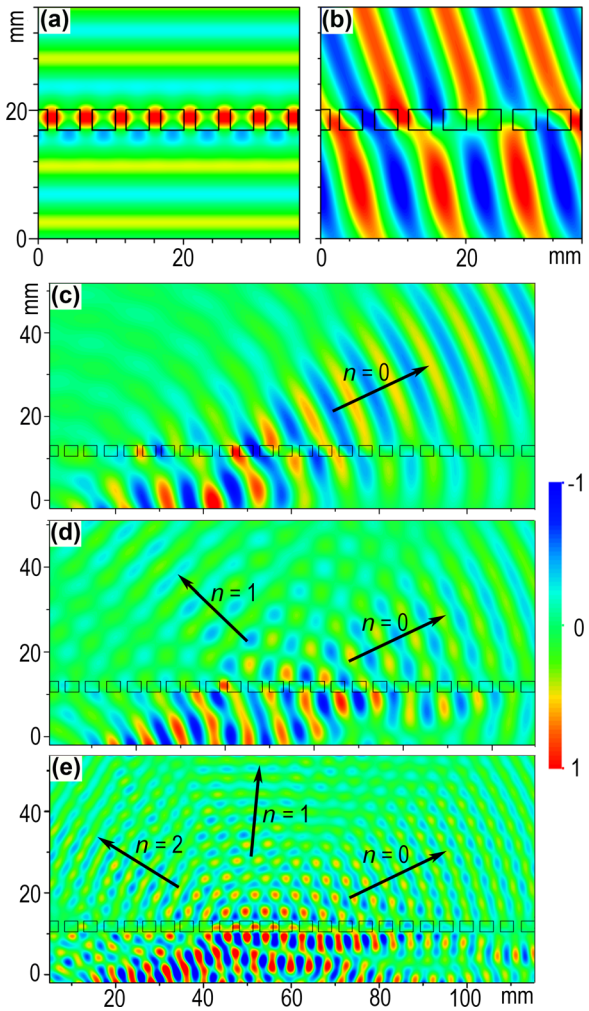

FIG. 3. (a) and (b) show the spatial intensity distribution of the pressure field (under periodic boundary) at high-transmission frequencies under different incident angles. (a) Normal incidence ($\theta = 0$) at $\omega = 47$ kHz; (b) the optimal incidence ($\theta = 72°$) at $\omega = 34$ kHz. For the optimal incidence ($\theta = 72°$), (c), (d), and (f) illustrate the spatial intensity distribution of the pressure field (in the sample with 24 slits) at different frequencies $\omega = 34$ kHz, 47kHz, and 84 kHz, respectively, which belong to different bands for flat transmission. Please note that the intensity of the pressure field in (e) is enlarged to be twice. The grating has the period of the slits d = 4.5 mm, the width of the slit w = 1.4 mm, and the thickness h = 2.76 mm.

into the zero-order mode and the two diffraction modes. Thus, the high-order diffraction effect reduces the transmission efficiency. Generally, in the low-frequency region below the first Wood's anomaly, since far-field diffraction is absent and the wave energy is solely concentrated to zero-order mode, the observed forward transmission is extremely high, approaching 100% when the absorption is negligible. While in the high-frequency region, multiple-order diffractive modes are excited, and then the transmission is reduced.

To further elucidate the FP resonances and the flat transmission in the grating, here we use an analysis model based on rigorous coupling wave approximation (RCWA) method for acoustic transmission through gratings. This model has already been described by Lu *et al.*[19] The pressure field inside the grating is assumed as zero-order acoustic waveguide mode in the air slit surrounded by the steel walls. Above and below the grating, the pressure field is considered to be composition of the diffractive waves. Inside the slit the pressure field can be expressed as the zero-order rectangular

wave guide mode. Then, the zero-order transmittance can be expressed as[19]

$$T(\omega) \propto \left| f \cdot q(\omega) \cdot F(\omega) \cdot \mathrm{sinc}\left(\frac{\beta(\omega) \cdot w}{2}\right) \right|^2, \qquad (1)$$

where f is the filling ratio in the grating, and $q(\omega)$ and $\beta(\omega)$ are the wave vectors perpendicular and parallel to the grating, respectively. The enhancement factor of diffraction is $F(\omega) = [\Gamma_1{}^2\exp(jqh) - \Gamma_2{}^2\exp(-jqh)]^{-1}$, where Γ_1 and Γ_2 are the quantities that relate to the coupling between diffraction modes and guided modes in the system. Besides, the resonant factor is defined as $\gamma = (\Gamma_2/\Gamma_1)\exp(-jqh)$. More details have been given in Ref. 19.

As shown in Figs. 1 and 2, the zero-order transmission spectra predicted by the RCWA method are represented by the blue curves, which agree well with the experimental data (dark curves) and the finite-element simulations (red curves). This clearly justifies the analytical method.

Now we can use the analytical model to explore the physical origins of the above phenomena. We study the resonant factor γ and the enhancement factor of diffraction $F(\omega)$ for sample I as a function of the frequency for both normal- and oblique-incidence conditions. For normal incidence, the FP resonances should appear at the phase of γ, i.e., $\arg(\gamma) = m\pi$, where m is an integer (as shown in Fig. 4(a)). Indeed, the FP resonances occur at these frequencies when $F(\omega)$ becomes the maximum, as shown in Fig. 4(c). Here note that the second-order FP resonant peak is very weak because it is affected by the Wood's anomaly. The entire transmission results from the coupling of the waveguide mode in the slits and the composition of diffractive waves outside the grating. For the optimal oblique incidence of $\theta_f = 72°$, both the phase of γ and the factor of $F(\omega)$ monotonically change within each transmission band [Figs. 4(b) and 4(d)]. In particular, the factor of $F(\omega)$ becomes maximum and almost independent of the frequency within the low-frequency band (<40 kHz), which leads to high and flat transmission.

The mechanisms can also be explained by the acoustic impedance between the air and the grating. For a given incident angle θ, the acoustic impedance[33] is $Z_{air} = \rho_0 c_0/(d\cos\theta)$ in the air and $Z_{grating} = \rho_0 c_0/w$ in the grating, where ρ_0 and c_0 are the mass density and acoustic velocity in the air. When $Z_{air} = Z_{grating}$, the acoustic impedance between the air and the grating is matched, and the acoustic transmittance through the grating attain the maximum. Therefore, the optimal incident angle for maximal transmission can be expressed as

$$\theta_f = \cos^{-1}\left(\frac{w}{d}\right). \qquad (2)$$

For the above lattice parameters d = 4.5 mm and w = 1.4 mm in both samples, Eq. (2) gives $\theta_f = 71.7°$, which is very close to the above measured optimal angle $\theta_f = 72°$.

Finally, we show in Fig. 5 the calculated angular transmission spectra of acoustic waves for sample I. Obviously, the results obtained from the finite-element simulations and the RCWA methods are in good agreement. In particular, the multiple-band flat transmission can be clearly observed as "red," "yellow," and "blue" regions. Therefore, the EAT phenomenon through gratings, i.e., high and flat transmission within multiple frequency bands, are well verified and understood.

In summary, we have experimentally and theoretically demonstrated that extremely high and flat transmission of acoustic waves within multiple frequency bands can be achieved through metallic gratings under oblique incidence. In general, the acoustic transmission properties depend on the coupling of diffractive surface waves and the waveguide modes. For small incident angles, the FP resonance mechanism dominates the resonant transmission peaks. For optimal oblique incidence, the impedance matching mechanism plays an important role. Under this condition, broadband full transmission (100%) can be obtained in the long wavelength range above the first Wood's anomaly, while in the shorter-wavelength ranges below the first Wood's anomaly, the grating has lower transmission due to the diffraction effect, but the transmission pattern still consists of nearly flat segments separated by the Wood's anomalies. Under the condition of

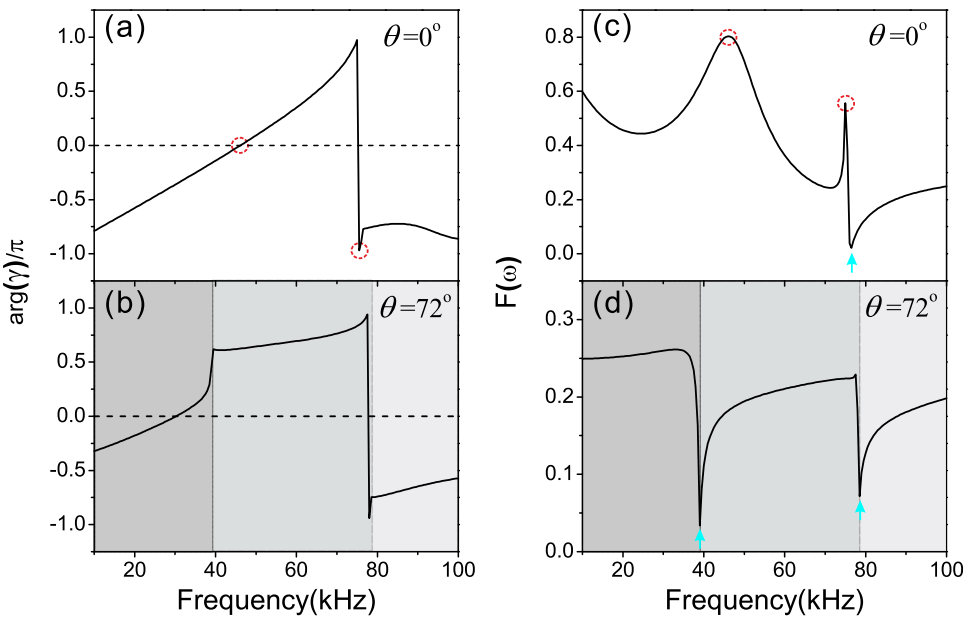

FIG. 4. The left panel shows the phase of the resonant factor γ in the grating as a function of frequency at different incident angles: (a) $\theta = 0°$; and (b) $\theta = 72°$. The right panel shows the enhancement factor of diffraction F(ω) in the grating as a function of frequency at different incident angles: (c) $\theta = 0°$; and (d) $\theta = 72°$. The grating has the period of the slits d = 4.5 mm, the width of the slit w = 1.4 mm, and the thickness h = 2.76 mm.

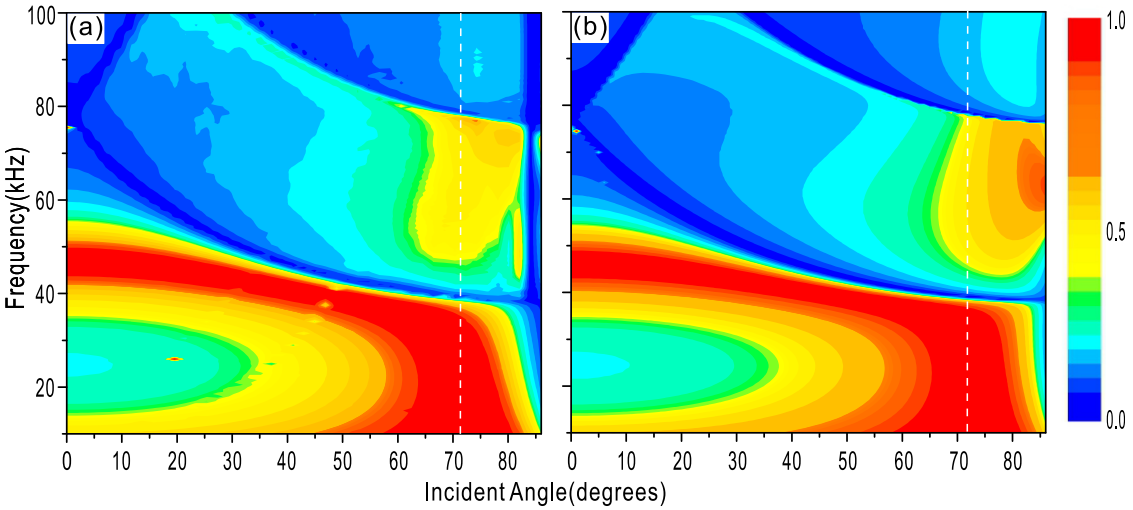

FIG. 5. The calculated angular transmission spectra of acoustic waves through the grating based on the following method: (a) the finite-element simulation and (b) the RCWA method. The white dashed lines indicate the optimal incident angle $\theta_f = 71.7^\circ$. The grating has the period of the slits d = 4.5 mm, the width of the slit w = 1.4 mm, and the thickness h = 2.76 mm.

low absorption, the transmission efficiency is nearly insensitive to the thickness of the grating. We can expect that if many gratings are stacked to obtain a sonic crystal, the acoustic impedance between this sonic crystal and the air are still matched for an optimal incidence angle, thus the extremely flat acoustic transmission with broadband frequency range will still exist for optimal oblique incidence. This work may open up a field for various potential applications of acoustic gratings, including broadband sonic imaging and screening, grating interferometry, and antireflection cloaking.

This work was supported by the Ministry of Science and Technology of China (Grant Nos. 2012CB921502 and 2010CB630705), the National Science Foundation of China (Grant Nos. 11034005, 61077023, 50972057, and 11021403), and partly by Jiangsu Province (BK2008012) and the Ministry of Education of China (20100091110029). X.R.H. was supported by the U.S. Department of Energy, Office of Science, Office of Basic Energy Sciences, under Contract No. DE-AC02-06CH11357.

[1]Y. M. Liu, and X. Zhang, Chem. Soc. Rev. **40**, 2494 (2011).
[2]J. B. Pendry, D. Schrurig, and D. R. Smith, Science **312**, 1780 (2006).
[3]R. A. Shelby, D. R. Smith, and S. Schultz, Science **292**, 77 (2001).
[4]J. B. Pendry, Phys. Rev. Lett. **85**, 3966 (2000).
[5]X. Zhang and Z. W. Liu, Nature Mater. **7**, 435 (2008).
[6]T. W. Ebbesen, H. J. Lezec, H. F. Ghaemi, T. Thio, and P. A. Wolff, Nature **391**, 667 (1998).
[7]H. Liu and P. Lalanne, Nature **452**, 728 (2008).
[8]Y. J. Bao, R. W. Peng, D. J. Shu, M. Wang, X. Li, J. Shao, W. Lu, and N. B. Ming, Phys. Rev. Lett. **101**, 087401 (2008).
[9]X. R. Huang, R. W. Peng, and R. H. Fan, Phys. Rev. Lett. **105**, 243901 (2010).
[10]W. L. Barnes, A. Dereux, and T. W. Ebbesen, Nature **424**, 824 (2003).
[11]L. Martín-Moreno, F. J. García-Vidal, H. J. Lezec, K. M. Pellerin, T. Thio, J. B. Pendry, and T. W. Ebbesen, Phys. Rev. Lett. **86**, 1114 (2001).
[12]F. Gao, D. Li, R. W. Peng, Q. Hu, K. Wei, Q. J. Wang, Y. Y. Zhu, and Mu. Wang, Appl. Phys. Lett. **95**, 011104 (2009).
[13]D. C. Skigin and R. A. Depine, Phys. Rev. Lett. **95**, 217402 (2005).
[14]S. Zhang, L. Yin, and N. Fang, Phys. Rev. Lett. **102**, 194301 (2009).
[15]N. Fang, D. Xi, J. Xu, M. Ambati, W. Srituravanich, C. Sun, and X. Zhang, Nature Mater. **5**, 452 (2006).
[16]J. Li, L. Fok, X. Yin, G. Bartal, and X. Zhang, Nature Mater. **8**, 931 (2009).
[17]T. Brunet, J.-L. Thomas, and R. Marchiano, Phys. Rev. Lett. **105**, 034301 (2010).
[18]H. Estrada, P. Candelas, A. Uris, F. Belmar, F. J. García de Abajo, and F. Meseguer, Phys. Rev. Lett. **101**, 084302 (2008).
[19]M. H. Lu, X. K. Liu, L. Feng, J. Li, C. P. Huang, Y. F. Chen, Y. Y. Zhu, S.-N. Zhu and N.-B. Ming, Phys. Rev. Lett. **99**, 174301(2007).
[20]Z. Liang and J. Li, Phys. Rev. Lett. **108**, 114301 (2012).
[21]J. Christensen, L. Martin-Moreno, and F. J. Garcia-Vidal, Phys. Rev. Lett. **101**, 014301 (2008).
[22]T. Still, W. Cheng, M. Retsch, R. Sainidou, J. Wang, U. Jonas, N. Stefanou, and G. Fytas, Phys. Rev. Lett. **100**, 194301 (2008).
[23]S. Zhang, C. Xia, and N. Fang, Phys. Rev. Lett. **106**, 024301 (2011).
[24]M. Farhat, S. Guenneau, and S. Enoch, Phys. Rev. Lett. **103**, 024301 (2009).
[25]B. Liu and J. P. Huang, Eur. Phys. J.: Appl. Phys. **48**, 20501 (2009).
[26]H. Chen and C. T. Chan, J. Phys. D: Appl. Phys. **43**, 113001 (2010).
[27]X. Zhu, B. Liang, W. Kan, X. Zou, and J. Cheng, Phys. Rev. Lett. **106**, 014301 (2011).
[28]A. Alù, G. D'Aguanno, N. Mattiucci, and M. J. Bloemer, Phys. Rev. Lett. **106**, 123902 (2011).
[29]R. H. Fan, R. W. Peng, X. R. Huang, J. Li, Y. Liu, Q. Hu, M. Wang, and X. Zhang, Adv. Mater. **24**, 1980 (2012).
[30]G. D'Aguanno, K. Q. Le, R. Trimm, A. Alù, N. Mattiucci, A. D. Mathias, N. Aközbek, and M. J. Bloemer, Sci. Rep. **2**, 340 (2012).
[31]N. Saiga and Y. Ichioka, Appl. Opt. **24**, 1459 (1985).
[32]J. R. Suckling, A. P. Hibbins, M. J. Lockyear, T. W. Preist, and J. R. Sambles, Phys. Rev. Lett. **92**, 147401 (2004).
[33]X. Wang, Appl. Phys. Lett. **96**, 134104 (2010).